Cloud Thermodynamic Models in Saturation Point Coordinates

ALAN K. BETTS

West Pawlet, VT 05775

(Manuscript received 16 February 1982, in final form 21 June 1982)

ABSTRACT

One-dimensional thermodynamic models for cloud-environment mixing, evaporation into downdrafts and precipitation from updrafts are presented in a parallel treatment using convective pressure scales and saturation point coordinates. This common framework can be used to interpret data sets and estimate from them pressure scales for the complex physical processes in cumulus.

1. Introduction

Betts (1982) introduced the saturation point (SP) representation of moist thermodynamics; showing how this unified our understanding of cloud processes in terms of conserved thermodynamic variables, simplified the representation of cloud-clear-air mixing processes and gave new insight into atmospheric mixing instabilities and thermodynamic equilibrium. The saturation point together with parcel pressure specifies the thermodynamic state of an air parcel whether unsaturated or cloudy (specifying cloud water but not precipitation) and can be regarded as a thermodynamic tracer. The purpose of this paper is to discuss simple one-dimensional thermodynamic models for cloud processes using this unifying SP approach. It might be thought that further analysis using one-dimensional models is anachronistic in view of the progress in the three-dimensional simulation of clouds (e.g., Miller, 1978; Klemp and Wilhelmson, 1978; Beniston and Sommeria, 1981). However, cloud processes both in the atmosphere and model simulations are so complex that their interpretation often requires simple bulk models. Furthermore, simple models are also necessary for the parameterization of cloud processes in the analysis of convective equilibrium structure and in large-scale numerical modelling. The models this paper will present are those for cloud–clear-air mixing or entrainment, droplet evaporation in unsaturated downdrafts, and precipitation fallout from updrafts using the SP framework and pressure scales as parameters for the different physical processes. The models themselves are not new, and there is much that remains unknown about the complex physical processes in clouds, but the common parametric framework presented here provides a more general framework for the consolidation of diverse data sets and the derivation of bulk parameters from them, as well as having clear advantages in teaching. Schematic thermodynamic diagrams will be used extensively for illustration. The representation of processes on these linearized diagrams gives an invaluable overview of the multitude of possible processes and how they might be combined, although more exact computations are needed for data analysis.

2. Cloud parcel paths and the saturation point

The main purpose of this section is to clarify the relationship between changes of SP and changes of thermodynamic invariables following parcel pressure p.

a. The SP coordinate system

The SP of an unsaturated (cloudy) air parcel is found by dry (moist) adiabatic ascent (descent) to the pressure level where the parcel is just saturated (with no cloud liquid water content) (Betts, 1982). At this saturation level (SL), the parcel temperature and pressure (T_{SL}, p_{SL}) uniquely specify the conserved parcel thermodynamic parameters (Betts, 1973) which are given symbols: θ_{SL}, θ_{ESL}, q_{SL}. For unsaturated air these are (θ, θ_E, q) and for cloudy air (θ_L, θ_{ES}, q_T),where $\theta_{(L)}$ denotes (liquid water) potential temperature, $\theta_{E(S)}$ (saturation) equivalent potential temperature, $q_{(S)}$ (saturation) water vapor mixing ratio, q_T total water and l cloud water (carried with air parcels until precipitated).

In dry or moist adiabatic motion, the parcel SP by definition does not change. Following a parcel we may write

$$\frac{dp_{SL}}{dt} = \frac{d\theta_{SL}}{dt} = \frac{d\theta_{ESL}}{dt} = \frac{dq_{SL}}{dt} = 0. \qquad (1)$$

We shall make the one-dimensional transformation $d/dt = \omega d/dp$ where $\omega = dp/dt$, and use the quasi-

0022-4928/82/102182-10$06.50

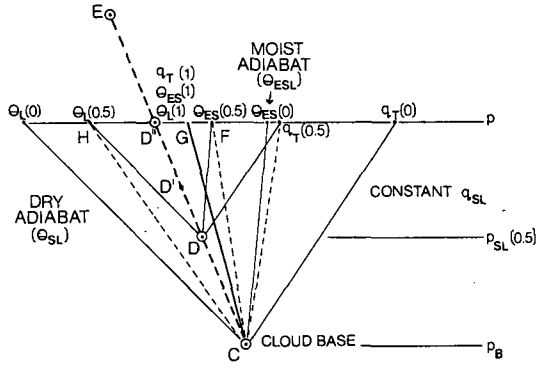

FIG. 1. Schematic tephigram showing relationship for cloud–clear-air mixing between change of saturation point and cloud parcel paths with respect to pressure. The heavy dashed line CE is the mixing line between cloud-base air and environmental air with SP at E. The light solid lines are dry and moist adiabats and lines of constant q. The light dashed lines are cloud parcel paths for $\beta = 0.5$. Numbers in parentheses denote values of β.

Lagrangian coordinates throughout, giving

$$\frac{dp_{SL}}{dp} = \frac{d\theta_{SL}}{dp} = \frac{d\theta_{ESL}}{dp} = \frac{dq_{SL}}{dp} = 0. \tag{2}$$

This paper will deal with processes which *change* parcel SP: mixing process, evaporation into downdrafts, and precipitation from updrafts. For these processes the SL, i.e., p_{SL}, changes, independently of parcel pressure p. To clarify the conceptually important relationship between derivatives with respect to p and p_{SL} we shall use the transformation

$$\frac{d}{dp} = \frac{dp_{SL}}{dp}\frac{d}{dp_{SL}} = \beta\frac{d}{dp_{SL}}, \tag{3}$$

giving dp_{SL}/dp the specific symbol β. This parameter interrelates parcel paths with respect to p and p_{SL} on a thermodynamic diagram from a purely geometric viewpoint. It is helpful to understand this relationship before introducing other physical parameters for entrainment, evaporation, etc. The approximation will be made for illustrative purposes (accurate to $\lesssim$10% at warmer temperatures) that over small pressure intervals, the gradients of the moist adiabat and mixing lines can be taken as constant, and a constant value of β will be considered.

The nonconserved thermodynamic variables, such as temperature, wet bulb temperature and dewpoint for unsaturated air, can always be recovered diagramatically by drawing the dry and moist adiabats and a constant q line through the SP to the parcel pressure p (e.g., through point D in Fig. 1).

b. *Mixing or entrainment into cumulus clouds*

The process of mixing of dry environmental air into cumulus clouds has been studied since the early work of Stommel (1947), who introduced the term *entrainment*. Fig. 1 shows this process of mixing in terms of the SP, following Betts (1982). The mixing of environmental air with SP at E into cloud with initial SP at C (corresponding to cloud-base air) moves the cloud parcel SP up a well-defined mixing line (CDD″) as the cloud parcel conserved thermodynamic parameters are changed by mixing. This simple case is not quite as restrictive as it first appears (i.e., corresponding to the mixing in of environmental air from only one level) since cumulus layers tend to have environmental SP's which themselves lie close to a well-defined mixing line.

As a cloud parcel ascends from cloudbase p_B to pressure level p, the degree of mixing determines how far its SP moves up the heavy dashed mixing line. The gradients following parcel pressure p can be written using (3) as

$$\frac{d\theta_{SL}}{dp} = \beta\left(\frac{d\theta_{SL}}{dp_{SL}}\right)_M, \tag{4a}$$

$$\frac{d\theta_{ESL}}{dp} = \beta\left(\frac{d\theta_{ESL}}{dp_{SL}}\right)_M, \tag{4b}$$

$$\frac{dq_{SL}}{dp} = \beta\left(\frac{dq_{SL}}{dp_{SL}}\right)_M, \tag{4c}$$

where the gradients suffixed M are those of the mixing line. The geometric and physical meaning of β in Fig. 1 is now apparent. $\beta = 0$ corresponds to no mixing so that the cloud parcel SP remains at C and cloud parcel paths follow the dry adiabat (θ_{SL}), moist adiabat (θ_{ESL}) and constant q_{SL} lines as p changes. $\beta = 1$ corresponds to mixing at such a rate that cloud liquid water just totally evaporates as a parcel ascends, so that $p = p_{SL}$ always. In this case the (cloud) parcel SP reaches D″ as the parcel reaches p, and the mixing line completely specifies all parcel thermodynamic parameters as it ascends. The range $0 < \beta < 1$ corresponds to partial evaporation of cloud water by mixing, which is typical of small cumulus. Fig. 1 shows parcel paths as functions of p for $\beta = 0.5$ as dashed lines. For example, from (4b), line CF, the cloud parcel path of θ_{ES} (and θ since it is saturated), lies halfway between the mixing line and the moist adiabat, while from (4a), line CH, the parcel θ_L path, lies halfway between the mixing line and the dry adiabat. During the ascent of the parcel from p_B to p, its SP has only moved halfway up the mixing line from C to D. Note that DH, DF are dry and moist adiabats, respectively. The mixing line and the single parameter β specify the gradients with respect to p of all cloud parcel thermodynamic parameters.

Cloud liquid water is of particular interest. For unmixed adiabatic ascent ($\beta = 0$) from cloud base p_B, liquid water (to the linear gradient approximation) is given by

$$l_A = (p_B - p)(\partial q_S/\partial p)_{\theta_{ES}}. \tag{5}$$

For ascent with mixing [Betts (1982), A5; or see the

difference in q_S on DF in Fig. 1]

$$l = (p_{SL} - p)(\partial q_S/\partial p)_{\theta_{ES}}. \tag{6}$$

Thus the ratio of l to the adiabatic value (for an *ascending* parcel) is

$$l/l_A = (p_{SL} - p)/(p_B - p) = 1 - \beta, \tag{7a}$$

since $\beta = (p_B - p_{SL})/(p_B - p)$. For an ascending parcel to remain cloudy clearly we require $l > 0$ and the mixing parameter $\beta < 1$.

There may be a more stringent buoyancy constraint on β. A schematic environmental stratification CG is shown on Fig. 1 (heavy solid line), corresponding to some mean $d\bar{\theta}_{ES}/dp$. For an ascending cloud parcel to remain buoyant (neglecting the θ_v correction for simplicity), its θ_{ES} and θ paths must lie to the right of CG, and its SP not reach D′ during the mixed ascent. For the environmental stratification CG shown, this requires

$$\beta < \frac{d\bar{\theta}_{ES}/dp}{(d\theta_{ESL}/dp_{SL})_M} \approx 0.7.$$

Thus with this environment, clouds that are just buoyant will have values of $l/l_A \approx 0.3$. Typical small clouds have measured values of l/l_A in this range (Warner 1970, 1977) so we see that their low liquid water content and marginal buoyancy are probably related to the environmental stratification (see Section 4).

Fig. 2 shows an illustrative example of parcel paths computed using a specified β and their relationship to a real sounding: an average tradewind sounding from BOMEX (22–24 June 1969; data supplied by E. Rasmusson). Cloud parcel paths have been plotted (light dashed lines) for $\beta = 0.6$ for a parcel rising from cloudbase (956 mb) to a cloud-top at 806 mb near the top of the trade inversion. It is presumed to mix continually with air entrained from cloud-top, and the mixing line is shown as a heavy dashed line (ABCE). This is the path of the cloud parcel SP. As the parcel rises 150 mb from cloud base to cloud top, its SP rises only 90 mb to 866 mb (point B). We have supposed the parcel to continue mixing, in some sense, at the same rate as it descends from cloud-top (it has overshot its equilibrium level), by setting $\beta = dp_{SL}/dp = -0.6$ on the descent. [The SL (p_{SL}) continues to move up the mixing line while p is now increasing.] The cloud parcel paths intersect at C where the parcel becomes unsaturated: its SL has risen from 866 to 843 mb as it has descended from cloud-top. The now cloud-free parcel will come to thermal equilibrium again (ignoring the θ_v correction) near 850 mb as shown, since θ_{SL} is now its potential temperature θ, while its SP has moved a little further up the mixing line to D, as mixing has continued.

For the cloud parcel paths shown, the ratio l/l_A on ascent is a constant 0.4 from (7), since β is constant;

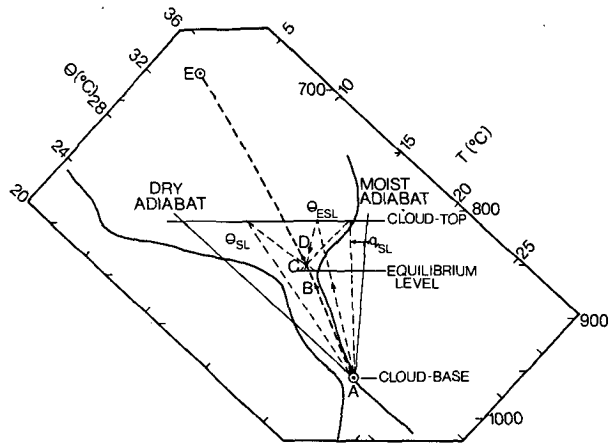

FIG. 2. Tephigram showing average tradewind sounding (heavy solid lines), mixing line between cloud-base and cloud-top environmental air (heavy dashed), and cloud parcel paths for $\beta = 0.6$ on ascent, $\beta = -0.6$ on descent (light dashed lines). B is the SP of cloud parcel at cloud-top.

whereas observational studies show l/l_A decreases with height (see Section 4), implying an increase of β. Fig. 2 illustrates clearly the marked asymmetry in the rate of change of cloud water between ascent and descent with mixing (Betts, 1973). If we define the saturation pressure difference

$$\mathcal{P} = p_{SL} - p$$

and note that $l \propto \mathcal{P}$ from (6), on ascent

$$d\mathcal{P}/dp = \beta - 1 = -0.4,$$

while on descent from cloud-top, when β has reversed sign,

$$d\mathcal{P}/dp = -1.6,$$

indicating the relatively rapid decrease of cloud water on descent.

The formula analogous to (7a) for cloud liquid water for a parcel *descending* from cloud-top (p_T) is

$$l/l_A = 1 - \beta\left[1 + \frac{2(p - p_T)}{(p_B - p)}\right], \tag{7b}$$

showing the reduced liquid water content, which decreases to zero as the cloud water all evaporates at a pressure level (here level C)

$$p_{EL} = \frac{(1-\beta)p_B + 2\beta p_T}{1+\beta} = p_T + \left(\frac{1-\beta}{1+\beta}\right)(p_B - p_T).$$

For $\beta = 0.6$, the descent distance for total evaporation is only one quarter, $(1 - \beta)/(1 + \beta)$, of the ascent from cloud-base to cloud-top.

c. *Evaporation into unsaturated downdrafts*

A simple model for this process was proposed by Kamburova and Ludlam (1966), and this was more recently extended by Betts and Silva Dias (1979). The

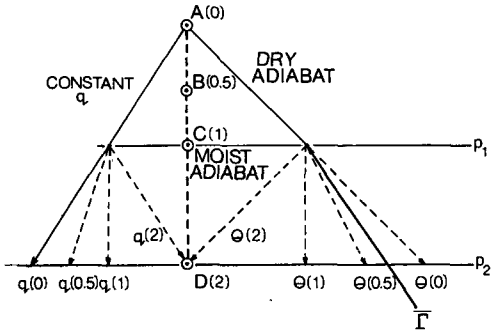

FIG. 3. Schematic tephigram showing relationship between change of SP and downdraft θ,q paths for different values of β (in parentheses). Downdraft SP descends moist adiabat as evaporation takes place. $\bar{\Gamma}$ indicates an environmental stratification.

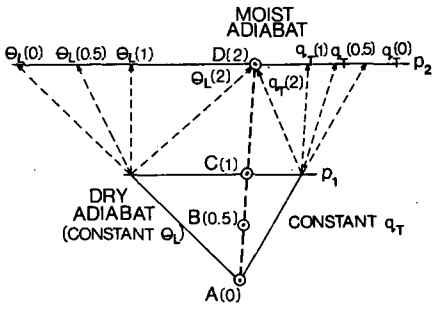

FIG. 4. Schematic tephigram showing relationship between change of SP and updraft θ_L, q_T paths for different values of β (in parentheses), in this case corresponding to different precipitation rates. Updraft SP remains on moist adiabat.

parameter β is again helpful in understanding the constraints on parcel paths in the evaporation process. In this case an air parcel SP is constrained to follow the moist adiabat (closely) corresponding to its initial θ_E (rather than a mixing line as in Section 2b). Now suppose that precipitation evaporates into a downdraft air parcel as it descends. Using (3) we may relate changes following parcel p and SP (p_{SL}), i.e.,

$$\frac{d\theta_{SL}}{dp} = \beta\left(\frac{d\theta_{SL}}{dp_{SL}}\right) = \beta\left(\frac{\partial\theta}{\partial p}\right)_{\theta_{ES}}, \tag{8a}$$

$$\frac{d\theta_{ESL}}{dp} = \beta\left(\frac{d\theta_{ESL}}{dp_{SL}}\right) = 0, \tag{8b}$$

$$\frac{dq_{SL}}{dp} = \beta\left(\frac{dq_{SL}}{dp_{SL}}\right) = \beta\left(\frac{\partial q_S}{\partial p}\right)_{\theta_{ES}}. \tag{8c}$$

Eq. (8b) follows from constant θ_{ESL} for the downdraft air, and (8a) and (8c) simplify because the gradients following the SP are just the gradients on the moist adiabat.

The physics implied by these expressions is clear if we consider conservation of θ_E on a downdraft trajectory,

$$\delta\theta_{ESL}/\theta_{ESL} = 0 = \delta\theta_{SL}/\theta_{SL} + L\delta q_{SL}/c_pT,$$

which relates the change of θ, the cooling, to the change of q, the evaporation. For a descent distance δp, and constant β,

$$\delta p_{SL} = \beta\delta p,$$

$$\frac{c_pT}{L\theta}\,\delta\theta_{SL} = \delta q_{SL} = \beta\left(\frac{\partial q_S}{\partial p}\right)_{\theta_{ES}}\delta p,$$

thus recovering (8c). Furthermore,

$$\delta\mathcal{P} = (\beta - 1)\delta p$$

so that for constant β, the downdraft saturation pressure difference $\mathcal{P}_d$ changes linearly with descent, i.e.,

$$\mathcal{P}_d = \mathcal{P}_I + (\beta - 1)(p - p_I), \tag{9a}$$

where the subscript I denotes values for the inflow to the downdraft at pressure level p_I.

The physical meaning of β is also clear (Fig. 3). $\beta = 0$ corresponds to no evaporation, no change of SP (remains at A), and the downdraft θ,q both remain constant. $0 < \beta < 1$ corresponds, for example, to a downdraft θ path between wet and dry adiabats, while the subsaturation, related to $\mathcal{P}_d$, increases linearly with descent. $\beta = 1$, corresponds to downdraft θ,q paths parallel to the moist adiabat, with constant subsaturation, and $\beta > 1$ to downdraft θ,q paths converging to saturation on the moist adiabat. Fig. 3 illustrates this by showing parcel θ,q paths for parcel descent from p_1 to p_2 corresponding to the descent of the SP from A to B, C, D for values of β of 0.5, 1.0, 2.0, respectively.

A parallel buoyancy constraint to the cumulus updraft may exist (Betts and Silva Dias, 1979). To maintain negative buoyancy a downdraft parcel must remain colder than the environment (if this can be defined near a thunderstorm!) which typically has a gradient between moist and dry adiabats: this implies β must be greater than a critical value. For the environmental $\bar{\Gamma}$ shown schematically, this would require

$$\beta > \bar{\Gamma}/\Gamma_W \approx 0.3,$$

where $\bar{\Gamma} = \partial\bar{\theta}/\partial p$ and $\Gamma_W = (\partial\theta/\partial p)_{\theta_{ES}}$. Typically $\bar{\Gamma}/\Gamma_W$ ranges from small values $\sim$0.2 for the severe storm atmosphere to $\sim$0.8 for some more stable tropical atmospheres. We would expect correspondingly a considerable range in downdraft characteristics (Betts and Silva Dias, 1979).

Eq. (9a) can be used to estimate a mean value of β from the end-points of a downdraft trajectory, where the suffices I, O denote downdraft inflow and outflow respectively; i.e.,

$$\beta = 1 + (\mathcal{P}_O - \mathcal{P}_I)/(p_O - p_I). \tag{9b}$$

d. Precipitation from updrafts

Diagrammatically the fallout of precipitation from updrafts is the inverse of Fig. 3, and the comparison

may be helpful. Again an updraft air parcel SP is constrained to lie on a moist adiabat (constant θ_{ESL}) while now θ_{SL}, q_{SL} change as cloud water is converted to precipitation and removed from an air parcel. Eqs. (8) are again satisfied, and β has a parallel physical meaning (Fig. 4). $\beta = 0$ corresponds to no precipitation and no change in SP (remains at A); $\beta = 1$ to all new condensate falling out so that cloud liquid water content remains constant (and SP moves from A to C as parcel goes from p_1 to p_2); and θ_L, q_T both parallel the moist adiabat; and $\beta > 1$ to precipitation falling out faster than more liquid condenses. Fig. 4 shows parcel (θ_L, q_T) paths for ascent from p_1 to p_2, corresponding to the ascent of SP from A to B, C, D for values of β of 0.5, 1.0, 2.0, respectively.

The parameter β in this case is the fractional fallout of new condensate, since

$$\frac{dl}{dp} = \frac{dq_{SL}}{dp} - \left(\frac{\partial q_S}{\partial p}\right)_{\theta_{ES}} = (\beta - 1)\left(\frac{\partial q_S}{\partial p}\right)_{\theta_{ES}}. \quad (10)$$

3. One-dimensional thermodynamic cloud models with convective pressure scales

The graphical approach using the parameter β clarifies some of the constraints on cloud thermodynamic processes. We shall now introduce parallel models using pressure scales for the largely unknown bulk physics of entrainment, droplet evaporation and precipitation. That we represent complex processes by single parameters reflects both our ignorance and the need to simplify for parametric and diagnostic purposes. There is some hope that these bulk pressure scales might be inferred diagnostically.

a. Mixing into cumulus

Bulk scales have been used by many authors to approximate entrainment into cumulus clouds (Simpson and Wiggert, 1969; Betts, 1973; Arakawa and Schubert 1974). For any conserved parameter such as θ_{ESL}, we can write (e.g., Betts, 1973)

$$\frac{d\theta_{ES}(c)}{dp} = \frac{\theta_{ES}(c) - \theta_E(e)}{\pi_M}, \quad (11)$$

where c, e denote cloud and environment, respectively, and π_M is a pressure scale for mixing into the cloud. If we also make a linear approximation to the mixing line (valid over small pressure ranges)

$$\frac{d\theta_{ES}(c)}{dp_{SL}} \approx \frac{\theta_{ES}(c) - \theta_E(e)}{p_{SL}(c) - p_{SL}(e)} = \frac{\Delta\theta_E}{\Delta\mathcal{P}}, \quad (12)$$

where $\Delta\theta_E$, $\Delta\mathcal{P}$ are shown in Fig. 5. We obtain from Eqs. (11) and (12) the approximate mixing relationship for $p_{SL}(c)$:

$$\beta = \frac{dp_{SL}(c)}{dp} \approx \frac{p_{SL}(c) - p_{SL}(e)}{\pi_M} = \frac{\mathcal{P}_c - \mathcal{P}_e}{\pi_M}, \quad (13)$$

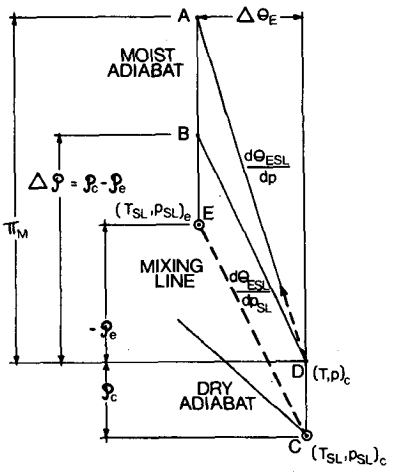

FIG. 5. Graphical construction of instantaneous updraft temperature path [Eq. (11)].

where $\mathcal{P}_c = p_{SL}(c) - p$ is the cloud saturation pressure difference.

Fig. 5 expresses (with linearized lapse rates) Eqs. (11), (12) and (13) graphically on a tephigram. CE is the instantaneous slope of the mixing line between cloud and environment. This is an instantaneous figure since the SP of the environment will in general change with height. The cloud parcel (which is above cloud base) has $(T, p)_c$ at D up the moist adiabat $\mathcal{P}_c$ (mb) from its SP at C. DB is drawn parallel to the mixing line, whose slope is $\Delta\theta_E/\Delta\mathcal{P}$, while DA, with slope $\Delta\theta_E/\pi_M$, is the instantaneous cloud parcel temperature (and θ_{ES}) path. The parameter $\beta = dp_{SL}(c)/dp$ in (13) is just the ratio of the slopes DA to DB in θ_{ES} coordinates. Earlier we gave β a value: now we shall consider the solutions of (13) obtained by specifying π_M.

1) LATERAL ENTRAINMENT

The familiar lateral entrainment model is given by taking π_M constant (mixing environment into the cloud as it ascends at a constant rate with pressure). $\mathcal{P}_e$ is related to the subsaturation of the environment [Betts, 1982, Eq. (A6)] which is typically near constant in a cumulus layer (see also Section 4). Taking π_M, $\mathcal{P}_e$ constant, (13) transforms readily to

$$\frac{d(\mathcal{P}_c - \mathcal{P}_e)}{dp} - \frac{\mathcal{P}_c - \mathcal{P}_e}{\pi_M} = -1, \quad (14)$$

with solution

$$\mathcal{P}_c = (\pi_M + \mathcal{P}_e)[1 - \exp(p^*/\pi_M)], \quad (15)$$

where $p^* = p - p_B$ is measured from cloud-base where $\mathcal{P}_c = 0$. The requirement for cloud water positive ($\mathcal{P}_c > 0$) requires

$$\pi_M > |\mathcal{P}_e|$$

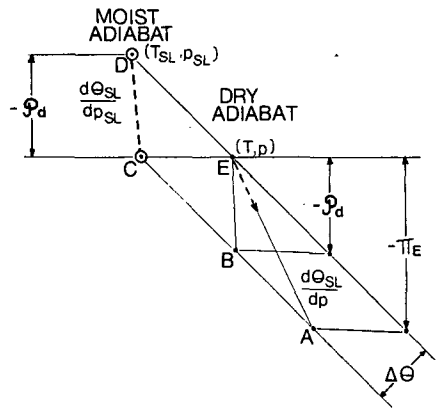

FIG. 6. Graphical construction of instantaneous downdraft temperature path [Eq. (19b)].

(since $\mathcal{P}_e$ is negative); that is, mixing must be less in drier environments for cloud to exist. Eq. (15) asymptotically approaches $\mathcal{P}_c = \pi_M + \mathcal{P}_e$, showing that cloud liquid water tends to a constant value

$$l_{\text{asym}} = (\pi_M + \mathcal{P}_e)(\partial q_s/\partial p)_{\theta_{ES}} . \tag{16}$$

In the asymptotic state, all variables θ_{SL}, q_{SL}, θ_{ESL} (and hence θ) for the cloud parcel instantaneously parallel the mixing line, and $\beta = 1$ (the parcel path DA in Fig. 5 becomes DB). We may think of π_M as the lag of the cloud parcel variables from those of the environment, which are changing with height (even though $\mathcal{P}_e$ is constant).

The ratio

$$l/l_A = -\mathcal{P}_c/p^* \tag{17}$$

decreases with ascent in accordance with observations. Expanding (15) for small p^*, we find that just above cloud-base

$$l/l_A = (\pi_M + \mathcal{P}_e)/\pi_M .$$

This ratio decreases as $|\mathcal{P}_e|$ approaches π_M. Just above cloud-base, $\beta = -\mathcal{P}_e/\pi_M$, but in this model β increases and approaches unity as a cloud parcel ascends.

We see from (16), (17) that cloud water measurements may be a simple indication of entrainment pressure scales, since $\mathcal{P}_e$ is observable.

2) CLOUD-TOP ENTRAINMENT

The entrainment of air through cloud-top was proposed by Squires (1958), and an observational example of cloud-top entrainment into Colorado cumuli was presented recently using a mixing diagram in Paluch (1979). From a mixing viewpoint this model has the advantage of simplicity in that air inside clouds is formed solely by mixing cloud-base air (from the subcloud layer) and cloud-top air. We may write (13) as

$$\frac{dp_{SL}(c)}{dp} = \frac{p_{SL}(c) - p_{SL}(t)}{\pi'_M} , \tag{18}$$

where $p_{SL}(t)$ is the SL of the environment at cloud-top and π'_M a pressure scale for cloud-top entrainment. Although $p_{SL}(t)$ may be considered constant, we have no expectation that π'_M should be constant as air parcels ascend through a cloud, and so simple integrations are not obvious.

b. Evaporation into downdrafts

Betts and Silva Dias (1979) have shown how droplet evaporation into unsaturated downdrafts can be represented parametrically by the pair of equations for the change of downdraft q, θ with pressure:

$$\frac{dq}{dp} = \frac{q - q_W}{\pi_E} , \quad \frac{d\theta}{dp} = \frac{\theta - \theta_W}{\pi_E} , \tag{19a, b}$$

where π_E is a pressure scale for evaporation[1] and the subscript W denotes values at the wet-bulb temperature. Using linearized gradients [(A1), (A5) of Betts, 1982]

$$\left.\begin{aligned} q - q_W &= \mathcal{P}_d\left(\frac{\partial qS}{\partial p}\right)_{\theta_{ES}} \\ \theta - \theta_W &= \mathcal{P}_d\left(\frac{\partial \theta}{\partial p}\right)_{\theta_{ES}} \end{aligned}\right\} , \tag{20a, b}$$

where $\mathcal{P}_d = p_{SL} - p$ for the downdraft air.[1] Substituting (20) in (19) and comparing with (8) yields

$$\beta = \frac{dp_{SL}}{dp} = \mathcal{P}_d/\pi_E . \tag{21}$$

The similarity to (13) is apparent: the difference comes from the fact that the downdraft SL is being changed by droplet evaporation at the wet-bulb temperature, rather than by the mixing in of dry environmental air as in the entraining updraft.

Fig. 6 shows the graphical construction of (19b) and (21). Instantaneously the downdraft has SP (T_{SL}, p_{SL}) at D and (T, p) at E. The downdraft SP follows the moist adiabat DC as evaporation takes place. DC and the parallel EB have linearized slopes $\Delta\theta/\mathcal{P}_d$, while the instantaneous downdraft temperature path from E follows EA with slope $\Delta\theta/\pi_E$, where $\Delta\theta = \theta - \theta_W$. The construction for the downdraft mixing ratio path is similar. The parameter $\beta = dp_{SL}/dp$ is just the ratio of the slopes EA to EB, as in Fig. 3. Eq. (21) can be rewritten as

$$\frac{d\mathcal{P}_d}{dp} - \mathcal{P}_d/\pi_E = -1, \tag{21b}$$

with solution for π_E constant

$$\mathcal{P}_d = \mathcal{P}_I \exp(p^*/\pi_E) + \pi_E[1 - \exp(p^*/\pi_E)], \tag{22}$$

where $\mathcal{P}_I$ is the saturation pressure difference of in-

[1] The sign convention of π_E, $\mathcal{P}_d$ is the reverse of Betts and Silva Dias (1979). Here both are negative.

flow air to the downdraft at pressure level p_I, and p^* is the descent $p - p_I$. We see that the initial condition $\mathcal{P}_I$ decays, and the downdraft $\mathcal{P}_d$ approaches π_E asymptotically (Betts and Silva Dias, 1979).

In terms of the parameter β, we see that the initial downdraft parcel paths (Fig. 3) are determined by the ratio $\mathcal{P}_I/\pi_E$, but if π_E is constant, $\mathcal{P}_d \rightarrow \pi_E$, $\beta \rightarrow 1$ and an asymptotic state is reached when downdraft θ, q both parallel the moist adiabat at constant subsaturation

$$q - q_W = \pi_E(\partial q_S/\partial p)_{\theta_{ES}}$$

given by (20a). Typical values of π_E are in the range 30–100 mb so that the asymptotic state is often approached. Thus the downdraft outflow saturation pressure difference $\mathcal{P}_O$ is often a good measure of π_E (Betts and Silva Dias, 1979). In general, a mean value of π_E can easily be derived from the end-points of a downdraft trajectory by rewriting (22) for the outflow as

$$\pi_E - \mathcal{P}_O = (\mathcal{P}_O - \mathcal{P}_I)/[1 - \exp(p_O^*/\pi_E]. \quad (23)$$

The first estimate of π_E is $\mathcal{P}_O$, and iteration is straightforward.

We may think of π_E again as a lag—a measure of how unsaturated a downdraft must be to evaporate droplets fast enough to maintain a constant subsaturation as the downdraft descends. It will increase with downdraft speed [cf. (30)] and as mean dropsize increases (Betts and Silva Dias, 1979).

c. *Precipitation from updrafts*

The microphysics of the processes that convert small cloud droplets to precipitation size particles are complex and change with parcel temperature, updraft speed and cloud life cycle to mention only a few variables. However, as was pointed out in Section 2c; the fallout of precipitation is in some thermodynamic aspects the inverse of evaporation into downdrafts, and a similar parametric approach may give some insight.

The simplest dimensional parameterization for precipitation is

$$\frac{dq_{SL}}{dp} = \frac{dq_T}{dp} = l/\pi_F, \quad (24)$$

where π_F is a pressure scale for the fallout of precipitation (e.g., the conversion of cloud water to rainwater). This has some physical basis in that most conversion processes are proportional to cloud liquid water content, and has been used in simple parametric models (e.g., Arakawa and Schubert, 1974). It is, however, oversimplified: for example, the pressure scale for autoconversion (for cloud updraft speeds of a few meters per second) is large [~200 mb (Kessler, 1969)], whereas for the accretion process once rainwater forms it is much smaller [≤50 mb (Kessler, 1969)]. Thus in a bulk sense it is no easier to predict π_F than π_E or π_M. From (24) and the linearized relationship

$$l = \mathcal{P}_c(\partial q_S/\partial p)_{\theta_{ES}}, \quad (25)$$

it follows, since the SP follows a moist adiabat, that

$$\beta = \frac{dp_{SL}}{dp} = \mathcal{P}_c/\pi_F. \quad (26)$$

Thus Eq. (26) can be represented graphically by a construction similar to Fig. 6 (inverted). From (26)

$$\frac{d\mathcal{P}_c}{dp} - \frac{\mathcal{P}_c}{\pi_F} = -1, \quad (27)$$

with solutions

$$\mathcal{P}_c = \pi_F[1 - \exp(p^*/\pi_F)], \quad (28)$$

where $p^* = p - p_B$ is the ascent from cloud-base p_B where $\mathcal{P}_c = 0$. We see as expected that $\mathcal{P}_c$ asymptotically approaches π_F when cloud water

$$l' = \pi_F(\partial q_S/\partial p)_{\theta_{ES}}. \quad (29)$$

Here $\pi_F \approx 50$ mb, $l \approx 1$ g Kg^{-1} at warm temperatures. In precipitating clouds we might thus regard the remaining cloud water as a bulk estimate of the pressure scale for precipitation fallout (π_F).

We see from (26) that β is zero at cloud-base but increases to 1 (for constant π_F), when the parcel paths of θ_L, q_T parallel the wet adiabat (Fig. 4). Cloud water then satisfies (29) and is precipitated as fast as it is condensed.

The pressure scale π_F is related to a timescale τ_F for the precipitation conversion by the updraft vertical velocity w, i.e.,

$$\pi_F = \rho g w \tau_F. \quad (30)$$

Thus, if τ_F is constant, π_F will increase with updraft speed, and hence so will l'.

4. Comparison of entrainment model and data

Of the three bulk parameters π_M, π_E, π_F, we shall take π_M for further illustrative study. The estimation of π_E from downdraft outflow data has been addressed in Betts and Silva Dias (1979), and the usefulness of π_F needs further study.

A simple comparison between the model and in-cloud measurements of liquid water will illustrate how entrainment parameters can be estimated and inferences drawn about entrainment into cumulus clouds. The processes of lateral and cloud-top entrainment give very different estimates of π_M, as well as different cloud parcel paths on a thermodynamic diagram, which may be used to distinguish which process may be dominant. We shall use the data of Warner (1970) discussed further in Cotton (1975) and Cotton and Tripoli (1978). This analysis will also cast

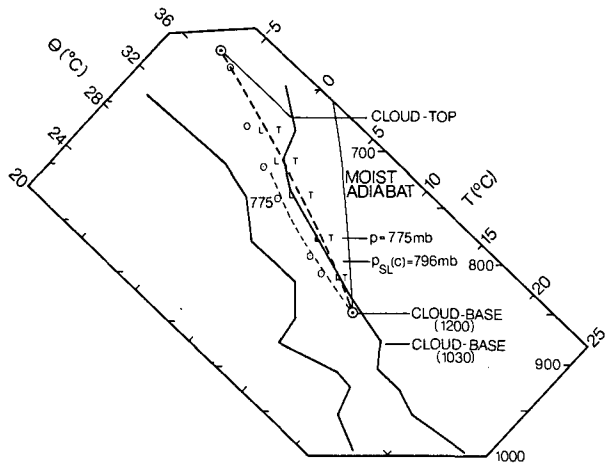

FIG. 7. Sounding at Bundaberg, Queensland, 10 November 1964 (solid lines). Heavy dashed line is mixing line with cloud-top entrainment, light dashed line with lateral entrainment, and symbols T, L denote cloud parcel temperatures for lateral and cloud-top entrainment, respectively.

some light on the dispute (Warner, 1970; Simpson, 1971) over whether one-dimensional models with lateral entrainment can simulate both cloud liquid water contents and cloud-top heights. Fig. 7 shows the sounding (solid lines) at Bundaberg, Queensland as constructed by Cotton (1975). Cloud-base at 1200 EDT was at 845 mb and cloud-top near 670 mb for a population of scattered cumulus. Environmental SP's corresponding to each data level in the cloud layer are shown as open circles. Various cloud parcel parameters are shown which will be discussed in Section 4b.

a. Estimation of π_M for lateral entrainment model

Fig. 8 shows a comparison between Warner's (1970) mean in-cloud values of l/l_A (solid line) with those computed with the simple lateral entrainment model (15), (17) using a constant value of $\mathcal{P}_e$ = 30 mb representative of the cloud layer for the Bunaberg sounding, and values of π_M of 50, 60, 70 mb. The agreement between data and model for π_M = 60 mb is quite satisfactory showing that the lateral entrainment model can give a realistic l/l_A decreasing with height above cloud-base, and that an observed profile gives an estimate of π_M. In this case π_M is about one-third of the total depth of cloud layer (175 mb). However, we shall see, as Warner (1970) concluded, that the corresponding cloud buoyancies with lateral entrainment matched to observed cloud liquid water are too low to give the observed cloud-tops.

b. Cloud parcel paths

Fig. 7 also shows paths of cloud parcel temperature and SP for lateral and cloud-top mixing. These depend on the cloud-base temperature (i.e., SP). The subcloud layer sounding is clearly not representative of cloud-base air, so the cloud-base SP has been taken as 0.5°C colder than the environmental temperature at the observed cloud base of 845 mb, consistent with other studies (Betts, 1976). The light dashed line is the path of a cloud parcel SP with lateral entrainment, computed from (12) and (15) using π_M = 60 mb. Cloud parcel temperatures for lateral entrainment are plotted as L's: they lie up the moist adiabat from the corresponding SP on the mixing line. The SP's of environmental air and cloud parcel (p_{SL} = 796 mb) at 775 mb are shown. The parcel temperature path traced by the L symbols lies close to the environmental temperature. Even with the θ_v correction, parcels with this lateral entrainment (corresponding to the observed l/l_A profile) are near neutral buoyancy and cannot ascend to the observed cloud-top height of 670 mb. As Warner (1970) and Cotton (1975) concluded, if the lateral entrainment rate is set to give observed cloud water, cloud-top heights will be greatly underpredicted.

Fig. 7 shows that cloud-top mixing gives a different result. The heavy dashed mixing line is the path of SP for the mixing of cloud-base air with cloud-top air. It lies close to the environmental temperature. Cloud parcel temperatures corresponding to cloud-top entrainment and the *observed mean values* of cloud water are plotted with the symbol T: these again lie $\mathcal{P}_c$[mb] up the moist adiabat from their corresponding SP on the cloud-top mixing line. We see that if the dominant entrainment process is at cloud-top, cloud parcels can have the *same* liquid water

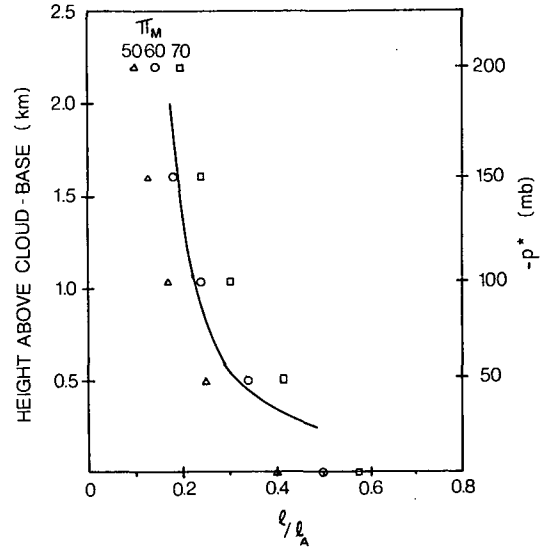

FIG. 8. Comparison of Warner (1970) mean cloud liquid water content (solid line) with model values computed using (15) with $\mathcal{P}_e$ = 30 mb, π_M = 50, 60, 70 mb, showing good agreement for π_M = 60 mb.

content as with lateral entrainment, but have much greater buoyancy and readily attain the observed top heights. This is a purely thermodynamic effect, associated with the SP structure of the environment (which is typical of other examples).

Values of π'_M computed from (18) for the observed Warner cloud water profile are much larger than π_M, corresponding to less mixing in of the drier cloud-top air. The computed π'_M decreases from ~300 mb near cloud base to ~100 mb at 700 mb. Thus, the use of a constant π'_M in (18) would not give a satisfactory profile of cloud water with height. [This reduced mixing rate (larger π'_M) would in some one-dimensional models, with drag terms in the momentum equation dependent on entrainment rate, further increase predicted cloud-top height.]

c. *Role of different entrainment mechanisms*

It is clear that in-cloud measurements of SP, requiring cloud temperature and liquid or total water measurements, will distinguish originating levels of entrained air, as in Paluch (1979). Because the environmental SP values typically lie to the left of the mixing line between cloud-top and cloud-base air, the cloud-top mixing process will tend to give more buoyant clouds for the same liquid water content.

Fig. 7 has an interesting symmetry which suggests that both lateral and cloud-top entrainment are important processes but they represent extremes. For *lateral* entrainment, the mixing line is to the left of the environmental temperature, so that cold downdrafts produced by evaporative mixing are possible (Betts, 1982), while the cloud parcel temperatures (marked L) indicate that updrafts are near neutral buoyancy. For *cloud-top* entrainment the cloud parcel temperatures (marked T) indicate strong buoyancy for updrafts, while the mixing line lies close to the temperature sounding, indicating that even with continuous evaporative mixing, downdrafts will be near neutral buoyancy.

Since we require buoyant updrafts to produce clouds, and negatively buoyant downdrafts if cloud-top environmental air is to be brought down into a cloud, it seems likely that both processes must play a role. A combination of lateral and cloud-top entrainment probably occurs so that both updrafts and downdrafts have significant available potential energy.

Heymsfield *et al.* (1978), Cotton and Tripoli (1979) and Tripoli and Cotton (1980) have discussed entrainment into cumulus in sheared flow. They suggest that the updraft grows with reduced entrainment on the upshear side of the cloud, while dry air is strongly entrained into a wake in middle and upper levels on the down-shear side producing a penetrating downdraft circulation. Fig. 7 shows that entrainment of dry air into a cloud wake from at and below the θ_{ES} minimum in the cumulus layer (705 mb in Fig. 7) rather than cloud top is more favorable for negatively buoyant downdrafts, since the environmental SP's lie to the left of the cloud-top mixing line. Air descending in these downdrafts might then mix with the updraft core on the upshear side of a cloud. This combination of processes would give both negatively buoyant downdrafts and buoyant updrafts, with a bulk entrainment process intermediate between the lateral and cloud-top models. The inference of empirical relationships for π_M from data using (13) would be useful.

5. Conclusions

This paper has presented a parallel development of one-dimensional thermodynamic models in saturation point coordinates. Model solutions using bulk parameters for the processes of entrainment, evaporation into downdrafts and precipitation in cumulus indicate how these parameters might be estimated from observational data sets. The pressure scale π_M for mixing or entrainment can be estimated from cloud-water measurements in shallow non-precipitating clouds, although the estimates are sensitive to the level of origin of entrained environmental air. This treatment clarifies the relationship of estimates of π_M to the environmental saturation pressure difference $\mathcal{P}_e$. The evaporation pressure scale π_E can be estimated from the saturation level of downdraft outflows, and the pressure scale π_F for the fallout of precipitation from cloud-water measurements in precipitating clouds. Where sufficient detail is available or needed, these models could be combined. Although much remains unknown about the complex processes in clouds, these simplified treatments suggest procedures for data analysis and parametric modeling.

A more detailed case study of shallow clouds over Australia indicates that in-cloud measurements of temperature and liquid water will distinguish cloud-top from lateral entrainment: clouds entraining mainly at cloud top will be more buoyant for the same liquid water content. It also seems likely that both processes (or entrainment from middle levels) are important in the maintenance of both updraft and downdraft circulations in small cumulus.

This paper has developed a conceptual framework; clearly all three cloud processes need further study to explore the usefulness of these models.

Acknowledgments. This work was supported by the Atmospheric Sciences Section (Global Atmospheric Research Program) of the National Science Foundation under Grants ATM-7915788 and ATM-8120444. I am grateful to the students and faculty at the State University of New York, Albany, and the University of São Paulo, Brazil, for helpful discussions.

REFERENCES

Arakawa, A., and W. Schubert, 1974: Interaction of a cumulus ensemble with the large-scale environment. *J. Atmos. Sci.*, **31,** 674–701.

Beniston, M. G., and G. Sommeria, 1981: Use of a detailed planetary boundary layer model for parameterization purposes. *J. Atmos. Sci.*, **38,** 780–797.

Betts, A. K., 1973: Non-precipitating cumulus convection and its parameterization. *Quart. J. Roy. Meteor. Soc.*, **99,** 178–196.

——, 1976: Modelling subcloud layer structure and interaction with a shallow cumulus layer. *J. Atmos. Sci.*, **33,** 2363–2382.

——, 1982: Saturation point analysis of moist convective overturning. *J. Atmos. Sci.*, **39,** 1484–1505.

——, and M. F. Silva Dias, 1979: Unsaturated downdraft thermodynamics in cumulonimbus. *J. Atmos. Sci.*, **36,** 1061–1071.

Cotton, W. R., 1975: On parameterization of turbulent transport in cumulus clouds. *J. Atmos. Sci.*, **32,** 548–564.

——, and G. J. Tripoli, 1978: Cumulus convection in shear flow: three-dimensional experiments. *J. Atmos. Sci.*, **35,** 1503–1521.

——, and G. T. Tripoli, 1979: Reply to comments on Cotton and Tripoli (1978). *J. Atmos. Sci.*, **36,** 1610–1611.

Heymsfield, A. J., D. N. Johnson and J. E. Dye, 1978: Observations of moist adiabatic ascent in northeast Colorado cumulus congestus clouds. *J. Atmos. Sci.*, **35,** 1689–1703.

Kamburova, P. L., and F. H. Ludlam, 1966: Rainfall evaporation in thunderstorm downdrafts. *Quart. J. Roy. Meteor. Soc.*, **92,** 510–518.

Kessler, E., 1969: *On the Distribution and Continuity of Water Substance in Atmospheric Circulations. Meteor. Monogr.*, No. 32, Amer. Meteor. Soc., 84 pp.

Klemp, J. B., and R. B. Wilhelmson, 1978: The simulation of three-dimensional convective storm dynamics. *J. Atmos. Sci.*, **35,** 1070–1096.

Miller, M. J., 1978: The Hampstead storm: A numerical simulation of a quasi-stationary cumulonimbus system. *Quart. J. Roy. Meteor. Soc.*, **104,** 413–428.

Paluch, I. R., 1979: The entrainment mechanism in Colorado cumuli. *J. Atmos. Sci.*, **36,** 2467–2478.

Simpson, J., 1971: On cumulus entrainment and one-dimensional models. *J. Atmos. Sci.*, **28,** 449–455.

——, and V. Wiggert, 1969: Models of precipitating cumulus towers. *Mon. Wea. Rev.*, **97,** 471–489.

Squires, P., 1958: Penetrative downdraughts in cumuli. *Tellus*, **10,** 381–389.

Stommel, H., 1947: Entrainment of air into a cumulus cloud. *J. Meteor.*, **4,** 91–94.

Tripoli, G. T., and W. R. Cotton, 1980: A numerical investigation of several factors contributing to the observed variable intensity of deep convection over South Florida. *J. Appl. Meteor.*, **19,** 1037–1063.

Warner, J., 1970: On steady-state one-dimensional models of cumulus convection. *J. Atmos. Sci.*, **27,** 1035–1040.

——, 1977: Time variation of updraft and water content in small cumulus clouds. *J. Atmos. Sci.*, **34,** 1306–1312.